ADVANCED SUSTAINABLE SYSTEMS
www.advsustainsys.com

# Clean Carbon Cycle via High-Performing and Low-Cost Solar-Driven Production of Freshwater

*Valerio Mazzone, Marcella Bonifazi, Christof M. Aegerter, Aluizio M. Cruz, and Andrea Fratalocchi**

**While renewable power available worldwide costs increasingly less than the least expensive option based on fossil fuels, countries continue to increase their coal-fired capacity, which should conversely fall by 80% within a decade to limit global warming effects. To address the challenges to the implementation of such an aim, here, a path is explored that leverages on a previously unrecognized aspect of coal, opening to a new solar-driven carbon cycle that is environmentally friendly. By engineering the porosity matrix of coal into a suitably designed compressed volumetric structure, and by coupling it with a network of cotton fibers, it is possible to create a record performing device for freshwater production, with a desalination rate per raw material cost evaluated at 1.39 kg $h^{-1}$ $\$^{-1}$ at one sun intensity. This value is between two and three times higher than any other solar desalination device proposed to date. These results could envision a clean and socially sustainable cycle for carbon materials that, while enabling an enhanced water economy with global access to freshwater and sanitation, poses zero risks of reinjecting $CO_2$ into the environment through competing economies in the fossil's market.**

## 1. Introduction

The recent G20 has championed the framework of circular carbon economy (CCE) as an inclusive vision to address the current crisis of unregulated $CO_2$ emission levels, to mitigate climate change through an umbrella of "4Rs" that could reduce, reuse, recycle, and remove excessive carbon from the atmosphere.[1] At the core of CCE is a wide range of technologies, ranging from negative emissions to carbon capture/storage and natural climate solutions, which aim to establish clean energy transition pathways toward the Paris agreement.[2]

A significant challenge to implementing CCE's objectives lies in devising truly circular technologies, which do not allow $CO_2$ to re-enter the atmosphere through competing economies along the fossil chain. For example, this could happen if synthetic jet fuels produced by recycling environmental $CO_2$ supply energy to conventional engines, which do not block $CO_2$ emissions. This opens the question of whether it is possible to devise an adaptive path to the CCE that could combine cost-effective opportunities with social predisposition factors, providing new avenues in the fossil value's chain that could help address climate change while promoting environmental security.

According to the world forum,[3] the scarcity of freshwater represents one of the most imminent crises of our society, killing more than 8 million people per year from famine, poor health, and hygienic conditions. The United Nations (UN) estimates that in a few years, 1.8 billion people (almost one-fifth of the world's population) will lack access to freshwater, calling for new technologies that could address this problem.[4] Currently, the artificial production of freshwater relies on fossil-fuel powered and high-maintenance methods, such as reverse osmosis or underground water extraction, whose discharged brine is polluting oceans and severely undermining the planet's hydro-geological equilibrium.

Solar steam generation has recently shown great potential in devising a clean approach to purification and freshwater production, desalination, and wastewater treatment.[5–18,18–21] Currently, the best evaporation efficiency—not including costs—is at 3.2 $kg\ h^{-1}m^{-2}$ from 1 sun solar irradiation and reported for nanostructured gels.[18] However, the manufacturing of these materials is expensive and hinders industrial applications.

Nature-based solutions offer the opportunity to address cost issues while maintaining efficient performances. In this work, we implement a highly efficient, scalable solar water generator by using a bottom-down device made with natural coal and

V. Mazzone, M. Bonifazi, C. M. Aegerter
Physik-Institut
University of Zürich
Winterthurerstrasse 190, Zürich 8057, Switzerland
A. M. Cruz
PERA Complexity, B.V. (Processes for Evolutionary Complexity Research and Applications)
Hoogoorddreef 15, Amsterdam 1101 BA, The Netherlands
A. Fratalocchi
PRIMALIGHT
Faculty of Electrical Engineering
Applied Mathematics and Computational Science
King Abdullah University of Science and Technology - KAUST
Thuwal 23955-6900, Saudi Arabia
E-mail: andrea.fratalocchi@kaust.edu.sa

The ORCID identification number(s) for the author(s) of this article can be found under https://doi.org/10.1002/adsu.202100217.



**DOI: 10.1002/adsu.202100217**

cotton fibers. Water transportation is partially decoupled from solar-to-thermal conversion, allowing the direct optimization of each independent process for providing the best results. The performance of the device $[\eta_g]=[\frac{kg}{h\ sun\cdot\$}]$ measured in terms of kilograms of freshwater produced every hour at 1 sun illumination intensity and with 1 $ of raw material, is two times higher than the closest available competitor, represented by carbon-coated paper.[22] The high performance of this system result from the combination of a high desalination efficiency $\eta = 2.2\ kg\ h^{-1}\ m^{-2}$ at one sun, with inexpensive materials cost due to the large availability of coal reservoirs worldwide.[23]

The technology proposed in this work follows the G20 Energy Ministerial's endorsement on the CCE in the framework of Natural Based Solution (NBS),[1] representing a cost-effective, value-adding strategy to mitigate climate change. It contributes to reducing fossil's combustion, which is the most substantial cause of the human-made increase of $CO_2$ in the atmosphere,[24] channeling fossil value products into an enhanced water economy that could benefit the society by addressing the pressing crisis of water scarcity. The proposed technology also complies with social sustainability factors, as it suggests an avenue for employing fossil's value products in clean cycles. If with no risks of reinjecting $CO_2$ in the atmosphere through competing economy loops along the fossil chain.

## 2. Material and Sample Preparation

Coal, either in fossil form or human-made carbonized structures (charcoal), has many advantages for solar steam generation in terms of strong light absorption, worldwide availability, and low cost. The main disadvantage lies in its porosity, which is usually insufficient to guarantee adequate water transport for enhanced evaporation. To address this issue, we suitably engineer the material porosity to achieve good water transport while enhancing the material's absorption properties.

**Figure 1**a–c provides a 3D illustration of this process. It starts from a piece of carbonized organic material or fossil coal (Figure 1a), which is first powdered (Figure 1b) by industrial blending and then compressed into a carbonized compressed powder (CCP) (Figure 1c). Herein we manufactured CCP by using carbonized coconut shells, which are off-the-shelf available and inexpensive material that can be easily processed with scalable and industrially-ready equipment. The carbonized coconut shells powder is obtained after carbonization at 500–600° temperatures at resident time of 5 min, and is characterized by particles size of 500 μm. To further characterize the CCP material we conducted X-ray diffraction measurements and registered the corresponding spectrum (Figure S1, Supporting Information). Coal characteristic peaks are clearly observable at $2\theta = 20°$ and $2\theta = 40°$, referring respectively to (002) and (041) crystalline planes. The peaks of the analyzed sample are broader than the standard coal spectrum[25] due to the high degree of amorphous structures and defects. The CCP forms the core of a thermally isolated, two-stage steam generation device, illustrated in Figure 1d.

When used as a water desalination system, the CCP exploits the synergy between cotton fibers and carbonized powder. The former is a primary water transportation system inside the CCP, and the latter constitutes both a volumetric light absorber and a secondary liquid transportation system. In the device in Figure 1d, the water is first extracted from the bottom reservoir, reaching the CCP through the cotton channels emerging from a thermally insulating platform (Figure 1d, white substrate).

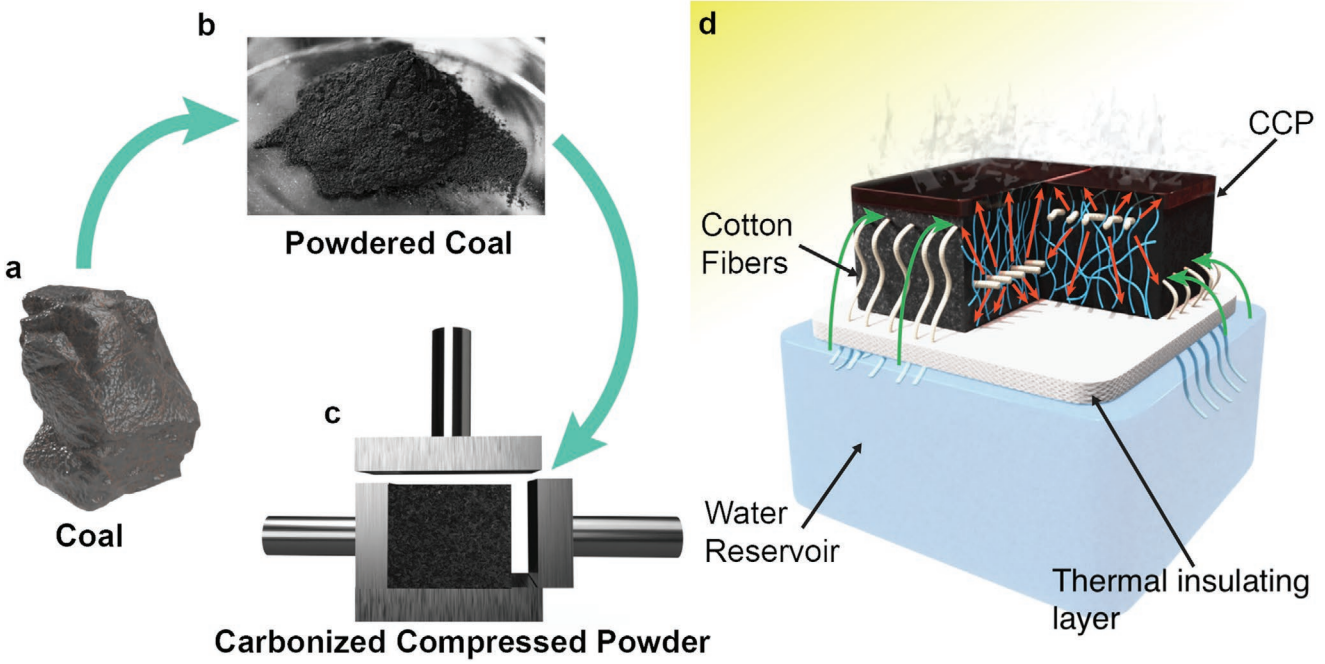


**Figure 1.** Fabrication process for production of carbonized compressed powder (CCP): a) a piece of fossil coal or organic carbonized material, b) is fine powdered by blending, and c) then compressed into an engineered carbonized compressed powder (CCP). d) Schematic of the solar absorber structure consisting of CCP and cotton fibers. The water is absorbed by the fibers (green arrows) and then distributed inside the CCP volume through a dense network of microchannels (red arrows and blue lines). A insulating layer guarantees thermal isolation between the bulk water and the CCP.

Water then diffuses inside the CCP through a complex network of micro-channels (Figure 1d, light blue lines). Capillary forces act on the liquid inside the CCP and transport the water from the bulk toward the upper surface and lateral walls (Figure 1d, red arrows), where broadband light absorption from the sun promotes the process of steam generation. Conversely to 2D structures, the device presented in Figure 1d is a 3D structure that absorb light from the top plane of the CCP, while the water-to-vapor conversion is carried out from all the surfaces exposed to air, allowing the device to go beyond the water-to-vapor conversion limit of 1.47 kg $m^{-2}$ $h^{-1}$. The use of cotton fiber as a primary water extract system isolates the CCP light absorber from the water, thus improving overall evaporation. By using a computer numerical control facility, we manufacture the holes in Figure 1d that accommodate the cotton fibers, passing the cotton across the gaps at different heights following perpendicular directions (Figure 1d). This approach guarantees a more considerable diffusion of water inside the CCP volume.

An essential benefit of CCP versus untreated coal lies in a higher water purification capability of the former. By powdering the coal and pressing it back together to form a bulk structure, it is possible to achieve a higher degree of porosity, with the net benefit of increasing the surface area available for adsorption of toxic compounds and other pollutants. In addition to that, by acting together with the CCP, the cotton fibers prevent organic and inorganic macro-molecules from being absorbed by the other thermally active part of the device, enabling freshwater production with low cost and high efficiency.

## 3. Sample Characterization

The ability of CCP to retain and distribute water depends on its complex porous network. This structure is created during the powdered phase within a rigid framework of disordered layers of carbon atoms, bonded together and unevenly stacked by chemical bonds that originate a highly porous structure of niches, cracks, and gaps within the carbon matrix. The porosity of CCP provides a large surface on which adsorption of a molecule can take place. Adsorption occurs by van der Waals and other attractive forces in pores that are slightly larger than the molecules to be adsorbed. Therefore, it is crucial to adapt the carbon network's pore size to the molecule to be adsorbed during the compression process. The fundamental properties that regulate adsorption in the CCP are the surface area, the total pore volume, and the pore radius.

**Figure 2**a shows an example image of the fabricated CCP samples, following the porosity engineering illustrated in Figure 1a–c. This treatment also has the beneficial effect of improving the optical absorbance of the carbon material, as demonstrated in Figure 2b by diffuse absorbance measurements with a control based on fossil charcoal[26] and carbonized wood (CW). The analysis reports that CCP behaves as a strong light absorber across a wide range of wavelengths, from 400 to 800 nm, reaching absorption values as high as 98.5 %. Figure 2b demonstrates that the CCP obtained with the optimization process of Figure 1 presents improved light-absorbing capabilities along the whole represented spectrum and quantified as 3% and 1.5% higher than carbonized wood and fossil charcoal respectively.

We study hydrophilicity properties of CCP by measuring the contact angle $\theta$ formed by a drop of water in contact with the CCP surface. We collect multiple measurements from different drops deposited in non-adjacent points of the surface of CCP blocks (see Figure S3, Supporting Information). The average value of $\theta$ is 49°, below $\theta_{limit} = 90°$, which is the threshold value adopted in the literature to discriminate between hydrophobic and hydropilic behaviors. It emerges from the measurements

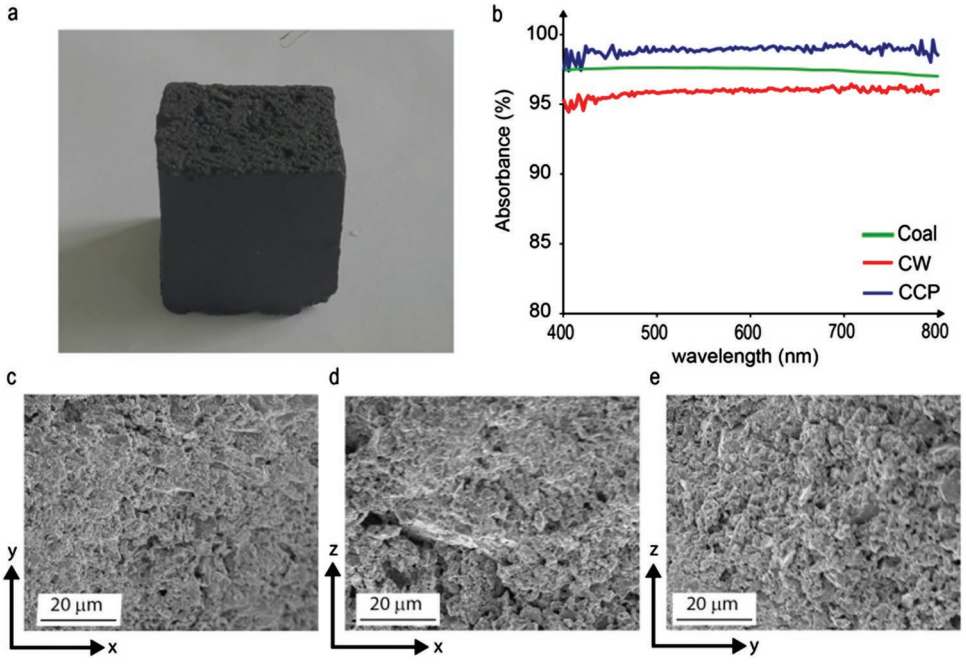


**Figure 2.** Material and optical characterization of CCP. a) Fabricated CCP cube 2.5×2.5×2.5 $cm^3$ b) Absorption spectra of fossil charcoal,[26] CW (carbonized wood) versus CCP. c–e) SEM images of CCP for orthogonal plane cross-sections.

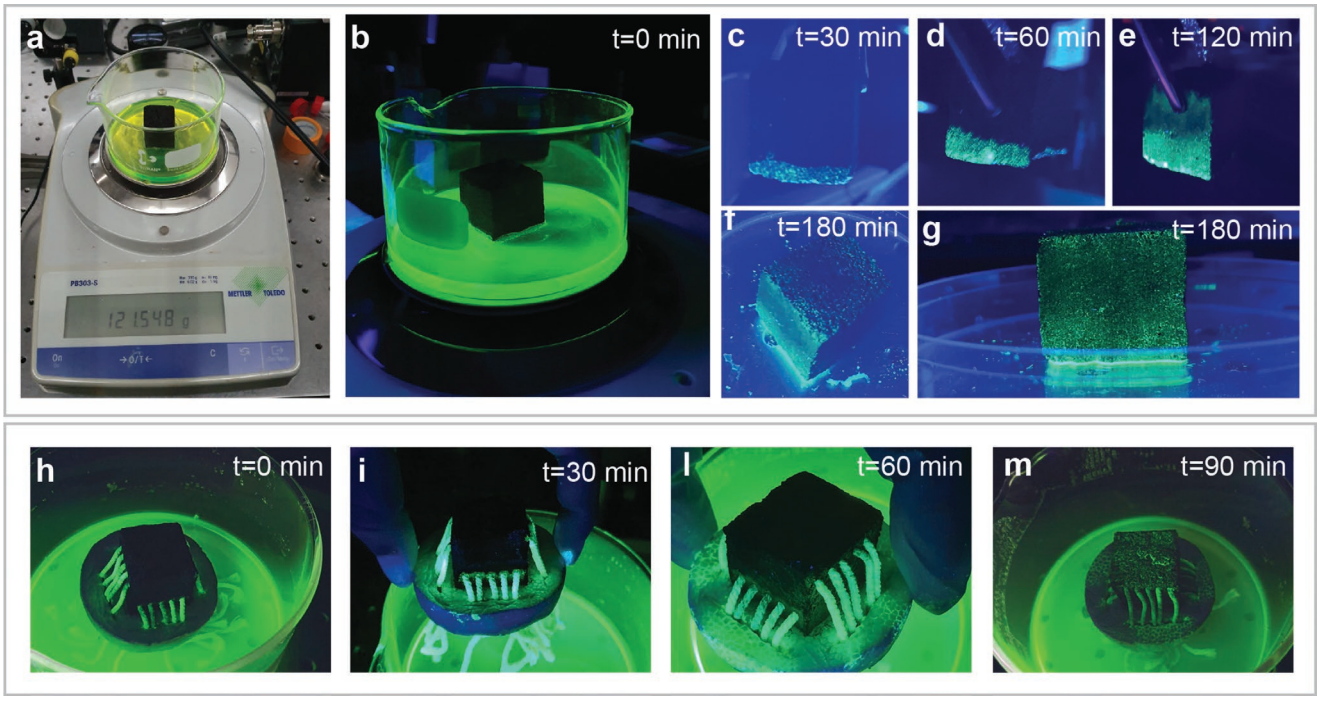


**Figure 3.** Characterization of CCP water absorption capability. a) Experimental set up to measure water absorbance and porosity. b–g) Time dynamic of the liquid absorption process inside CCP over 180 min. The ink level is made visible at every step though a UV lamp. h–m) Dynamic of liquid absorption in the device composed of CCP and the complex network of cotton fibers over 90 min. The system reaches saturation in half of the time with respect to the CCP with no fibers.

that cotton fibers does not influence the hydrophilicity of the CCP.

Figure 2c–e shows a morphology analysis of a CCP sample studied through scanning electron microscopy (SEM) with a Zeiss Supra 50 VP microscope along three different perpendicular cross-sections. The images show the same pores' distribution characterized by a complex network of micro-sized channels ranging from tens of microns to hundreds of nanometers. The SEM gray-scale images also provide information about the CCP porosity, defined as the ratio between the total volume occupied by the pores and the sample's overall volume. The porosity is quantitatively measured applying an image processing algorithm to the SEM images as described in ref. [27] and detailed in the Supporting Information (Section: Porosity Estimation).

This analysis shows that the CCP has an average porosity of 29.8%, with a standard deviation of 1.8%. The sub-micrometer pores radius varies within the range of 100–300 nm, with a porosity density of $153 \times 10^3$ pores $mm^{-2}$. Conversely, micrometer pores' radii lie between 2.4 and 5 μm, with a density of $10^3$ pores $mm^{-2}$. The analysis of Figure 2c–e shows that sub-micrometer pores are randomly distributed on the surface of the microchannels, constituting the openings for the nanochannels that spread in every direction, intercrossing other micro/nanochannels and shaping the highly interconnected disordered structure.

To confirm these measurement results, we use a liquid absorption method to absorb a marker liquid in the sample until saturation. When this occurs, the sample's weight stabilizes over time. The fluid volume inside the sample–and thus the porosity—is then calculated by subtracting the final weight from the sample's initial one. **Figure 3**a shows the setup used to measure the porosity values of the CCP. It consists of an analytical balance and a beaker. We fill the beaker with a contrast liquid composed of water and fluorescent ink to characterize the height at which the fluid flows over time. Figure 3b shows that at $t = 0$ the CCP is completely dry. Figure 3c–g illustrates the photo-sequence of the progressive absorption of contrast liquid through the CCP.

The liquid method returns a porosity value of 30%, which is in good agreement with SEM cross-sections measurements. Figure 3h–m replicates the experiments of Figure 3c–g on the CCP device embedded with cotton fibers. The addition of secondary cotton water extraction channels provides an enhanced factor of 100%, with the CCP saturated in half of the time than the cotton fibers-free configuration.

## 4. Indoor Experiment under 1 sun

**Figure 4**a illustrates the experimental setup used to test the CCP water evaporation device. It consists of a beaker filled with water, placed over an analytical balance, and insulated by aluminum foil. A computer continuously records the weight reported from the balance and measures the mass variation rate of water due to evaporation. We illuminate the device under 1 sun (1 kW $m^{-2}$) and use a thin insulating platform to thermally insulate the system (CCP and cotton fibers) from the water.

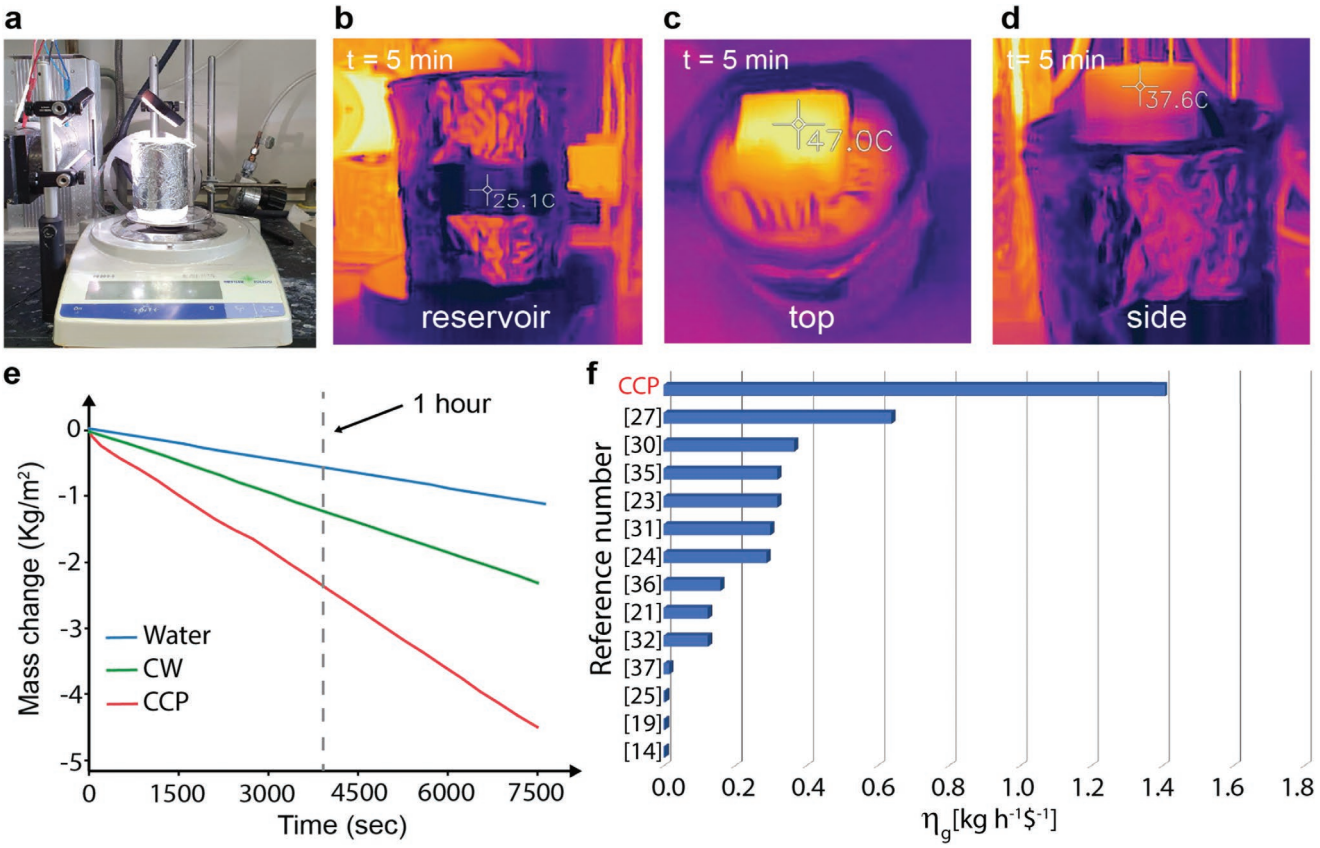


**Figure 4.** Indoor evaporation experiment. a) Optical setup with sun simulator to illuminate the structure, and balance to continuously measure the water mass change. b–d) Thermal images and temperature measurement of the water reservoir, charcoal top side, and charcoal lateral side, respectively. e) Comparison between the mass loss rate of water versus time under 1 sun illumination for bare water, carbonized wood, and engineered CCP with cotton fibers. f) Comparison of global efficiency $\eta_g$ defined as kg of freshwater produced per every hour, per every dollar ($) at one sun intensity of solar desalination devices available in the literature.

The cotton fibers are immersed in water on both sides of the CCP, going through the thermally insulating foam and channeling water into the CCP volume thanks to the CCP complex porous network's macro and nano-channels.

We use an infrared (IR) camera to continuously monitor the desalination system's temperature for the duration of the experiment (Figure 4b–d). Conversely, we monitor the water temperature inside the beaker through a window cut in the aluminum cladding (Figure 4a). Starting from a room temperature of 25 °C, after 5 min (300 s) the temperature of the top part of the device reaches 47 °C (Figure 4b) and 37 °C on the side (Figure 4c). During this phase, the water does not exhibit any appreciable temperature variation and stays constant around $T = 25$ °C.

Thanks to the presence of the cotton fibers as primary water transportation system, this device decouples efficiently the solar adsorber/evaporator from the seawater reservoir. In this system cotton fibers collects most of the salts presented in the water, preventing salt accumulation on the CCP surface. Being in continuous contact with water, fibers are always wet, thus avoiding clogging and loss in transport efficiency. In our studies, we were able to use the same CCP block for four consecutive weeks, observing no significant loss of performance.

Figure 4e reports the results of mass evaporation rate over time. Bare water presents an evaporation rate of $m_{H_2O} = 0.36 \text{Kg m}^{-2} \text{ h}^{-1}$, while standard carbonized wood (CW) directly immersed in water and thermally insulated on the sides produces a mass change rate of $m_{cw} = 1.1 \text{ Kg m}^{-2} \text{ h}^{-1}$ (Figure 4e, green line). The CCP device shows a much higher evaporation rate equal to $m_{ccp} = 2.2 \text{ Kg m}^{-2} \text{ h}^{-1}$, for a total mass change of 4.4 Kg $\text{m}^{-2}$ in 2 h (Figure 4e, red line).

We calculate the evaporation efficiency of CCP applying the established formula[28] derived form the equation of energy balance:

$$\eta = \frac{\dot{m} h_{LV}}{P_{in}} \tag{1}$$

and followed the measurement process explained in ref. [29] for volumetric absorbers. As described in ref. [15,16], high-performing 3D evaporators can overcome the theoretical limit of evaporation rate 1.47 $\text{kg/m}^{-2} \text{ h}^{-1}$ calculated for 2D systems. In this case, this is due to an increase in evaporation surface, considering the evaporation process happening from the illuminated top side as well as from the non-illuminated sidewalls. In addition, due to its porous nature, water evaporation enthalpy is reduced[18] and the intrinsic evaporation ability of

CCP is increased respect to pure water. When this condition occurs, the efficiency of the volumetric evaporator exceeds the value of 100%, which corresponds to the maximal efficiency of a 2D evaporator at the evaporation rate of 1.47 kg $m^{-2}$ $h^{-1}$. The system proposed in this work reports an evaporation rate of 2.2 kg $m^{-2}$ $h^{-1}$, corresponding to an evaporation efficiency of 149% measured against the maximum value of 2D absorbers.

To quantify the performance of our device in light of industrial applications of solar steam generation, we calculated the desalination rate per material cost $\eta_g$:

$$\eta_g = \frac{\text{Kilograms of } H_2O \text{ evaporated}}{\text{hour} \times \$ \times \text{sun illumination}} \quad (2)$$

In the cost evaluation, we calculate the price of the materials for unit surface used in the various systems under consideration, obtaining a figure of merit that is independent of the device surface area, and directly dependent on the material costs in $. In the calculation of costs we did not include costs that are common to all described systems, and that cannot be quantified because they depends on factors that are unrelated to the system itself. These costs include, for example, preparation technology expenses such as electricity and labor, which vary according to time, location, quantity of processed materials, and cost of local man-power. The raw materials employed in each technology (e.g., coal, paper, wood, gold, cotton), on the contrary, define commodities whose costs are defined by standardized indices and on international suppliers/vendors websites, with fluctuations that are very small in both time and space. Table S1, Supporting Information shows a quantitative comparison of various state-of-the-art systems with a detailed breakdown of indoor/outdoor desalination efficiency, cost of raw materials, and combined desalination efficiency × cost of raw materials. These results show that raw costs impact each technology differently, with significant differences from one system to another (Figure 4f). The system presented in this work shows the highest evaporation rate per material cost, with 1.39 kg $h^{-1}$ $\$^{-1}$ at 1 sun intensity, more than two times higher than devices that use low-cost materials such as fiber-rich non-woven paper, cotton sheets, carbon nanotubes, and carbon nanoparticles (0.64,[22] 0.367,[30] 0.3,[31] 0.125 kg $h^{-1}$ $\$^{-1}$,[16,32] respectively), due to their lower evaporation rates.

## 5. Outdoor Experiment

We implement a 34 cm × 34 cm large CCP prototype for solar desalination and purification and place it near the seashore in King Abdullah University of Science and Technology (**Figure 5**a,b). The device encompasses a 20 cm × 20 cm area made of CCP interconnected with 640 cotton fibers, each of 20 cm length. The extremities of each fiber are immersed in the seawater collected directly from the Red Sea, and stored in a central reservoir at the bottom of the device. This ensures that water is continuously provided to the CCP for the duration of the experiment (Figure 5a). As shown in Figure 5b, purified water condenses onto the wall of the truncated-pyramid part of the device and is collected in the ring-shaped reservoir manufactured at the bottom.

The outside temperature, monitored during the experiment from 7 AM to 7 PM (Figure 5c), ranges between 28 and 37 °C. The average solar flux was 0.5 kW $m^{-2}$ with a peak of solar intensity of 0.950 kW $m^{-2}$ at 12 PM.

We conduct analytical measurements with specific probes on samples with Red Sea water and purified water from the outdoor experiment to attest the quality and the efficiency of the desalination process (Figure 5d–f). Salinity is decreased by 99.4%, dropping from 41 000 to 240 ppm, being well within the range of values for fresh potable water (salinity should be lower than 500 ppm, Figure 5d). The amount of total dissolved salts (TDS) dramatically decreased as well, from 42 000 to 355 ppm, well within range with the standard values for freshwater (TDS $<500$ ppm, Figure 5e). Finally, we perform water conductivity measurements of both water samples, observing a reduction from 50 000 to 420 μS in the purified sample, also well within acceptable values for potable water (between 150 to 500 μS). We used ICP mass spectroscopy to further confirm that freshwater resulting from the CCP evaporator is potable. We considered five primary ion species $Ca^{2+}$, $Mg^{2+}$, $K^+$, $Na^+$, $B^{3+}$, which are the typical most abundant ions in seawater. Figure S4, Supporting Information shows a comparison regarding the concentration level of the investigated primary ions present in the seawater sample before and after the desalination process. Their presence is strongly reduced and their final concentration is well below the limits established by the WHO and found in the literature.[33,34]

## 6. Discussion and Conclusions

We implemented and characterized a solar-driven water generator composed of carbonized compressed powder and cotton fibers. The device reported the highest global efficiency to date of 1.39 $kgh^{-1}$ $\$^{-1}$, measured in terms of kg of freshwater produced per hour and per $ spent on the material under 1 sun intensity. A typical coal-fired power station with an efficiency of 34% emits on average 1 kg of carbon dioxide for every 1 kWh of electric power produced.[35] When such electrical energy is used to power up traditional freshwater production systems based on, for example, reverse osmosis, highly concentrated brine is also generated in addition to the $CO_2$ injected in the environment, polluting both seas and oceans.

On the contrary, the system proposed in this work exploits coal in a clean solar-driven cycle that does not generate harmful byproducts, with an earth-abundant material that is widely available on many continents. The detrimental effects of water scarcity, indeed, result in the deterioration of human health and environmental conditions and affect local economies that rely on water for industry and agriculture. The financing of conventional water treatment plants often represents a barrier for development, especially in areas heavily affected by water shortage, which are usually poor, rural, or isolated.

The adoption of solar-driven CCP in water treatments could help the development of a decentralized economy for freshwater. Decentralization has several advantages, especially the possibility of placing plants near the source of supplies and

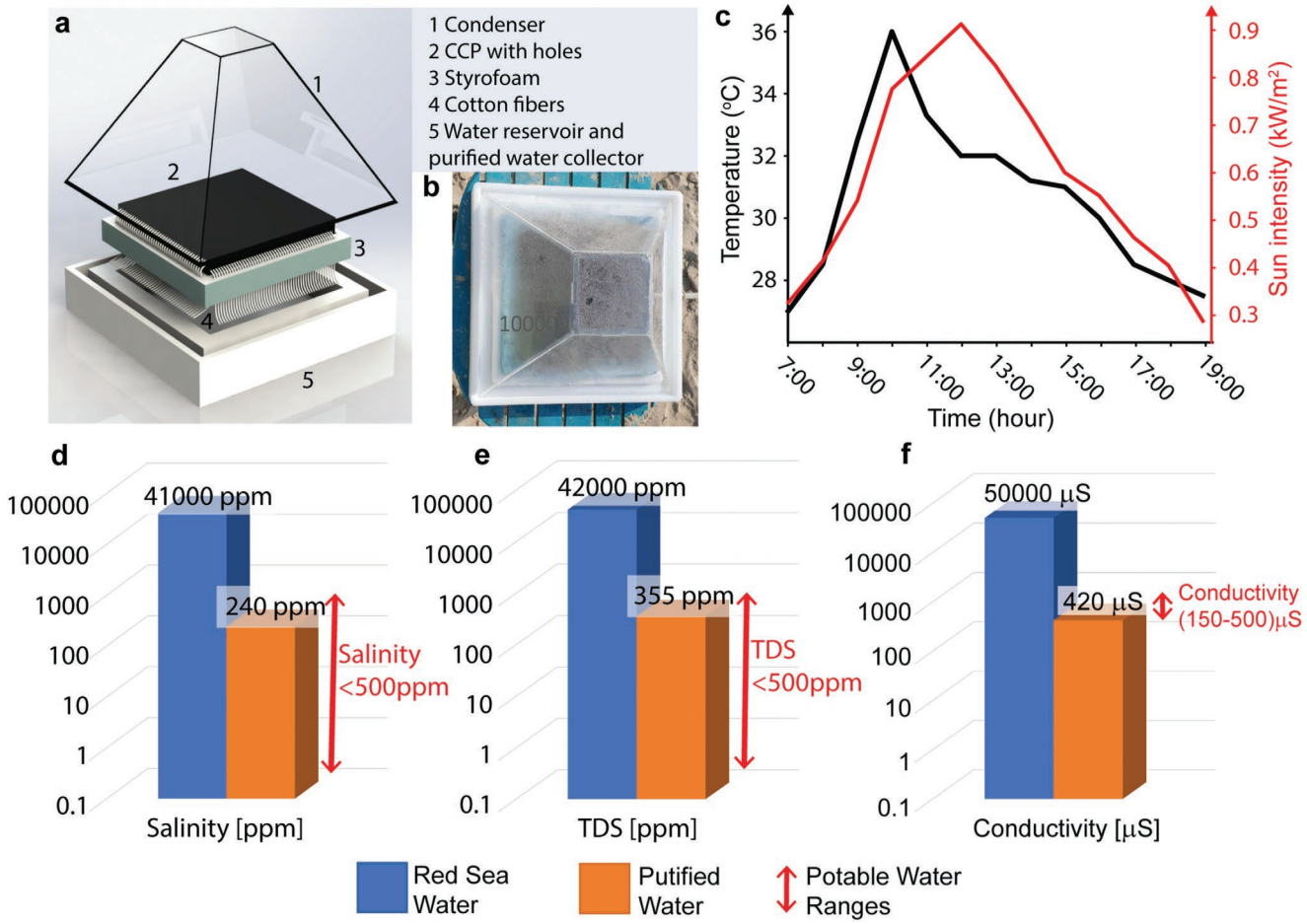


**Figure 5.** Outdoor experiments. a) Large scale system prototype: reservoir, CCP with cotton fibers, insulating layer and purified water collecting structure. b) Prototype during the experiment outdoor at King Abdullah University of Science and Technology, Jeddah (SA). c) Outdoor temperature and sun intensity tracking during the 12 h of the experiment. d–f) Comparison of values of d) salinity, e) total dissolved salts, and f) conductivity for Red Sea and purified water with the device in (a). Potable water ranges for each indicator are reported in red arrows.

financial convenience for smaller-scale realizations. According to the WHO (World Health Organization) guidelines, a primary water source should be at most 1000 m or 20 min away and should provide 20 L day$^{-1}$ per family member. With the system proposed in this work, a small-scale CCP with an 8 m$^2$ area can serve a family of four people, producing freshwater at the cost of around 0.002 \$ L$^{-1}$. This figure is already competitive with the average cost of water from reverse osmosis, evaluated at 0.0015 \$ L$^{-1}$,[36] without taking into account the cost of large-scale facility realization.

The use of coal resources for freshwater production can also address the continued erosion of coal's bottom line, which originated from the competition with other energy sources.[37] The electricity generated from coal has plateaued for almost a decade, and new coal-fired installations run at fewer hours since 2014.[38] For every GW of coal power that could be phased out by directing coal resources into an enhanced water economy, it would be possible to remove every hour more than 1000 tonnes of $CO_2$ from the environment. It could help favoring solutions for fossils' products that could attain the sustainable development goals of clean water, sanitation, and climate action.

## Supporting Information

Supporting Information is available from the Wiley Online Library or from the author.

## Acknowledgements

V.M. and M.B. contributed equally to this work. The authors acknowledge the financial support of PERA Complexity and the advisory support of co-founder Quelita Moreno. The authors acknowledge the support of the mechanical workshop of the Physics Department at University of Zurich (UZH) and of Prof. David Tilley and all the members of his research group at the Department of Chemistry of the University of Zurich (UZH).

## Conflict of Interest

A patent application number EP 20214979.5 has been filed to the European Patent Office on the basis of this discovery, with all authors of the manuscript listed as inventors.

## Data Availability Statement

Research data are not shared.

## Keywords

carbon emission reduction, solar desalination, sustainability, water economy

Received: July 7, 2021
Revised: August 11, 2021
Published online:

[1] T20 Statement on the Circular Carbon Economy, https://t20saudiarabia.org.sa/en/news/Pages/cce_statement.aspx (accessed: November 2020).
[2] (IEA), CCUS in Clean Energy Transitions **2020**, https://www.iea.org/reports/ccus-in-clean-energy-transitions (accessed: September 2020).
[3] Water.org, https://water.org/ (accessed: January 2021).
[4] H. D. R., Water scarcity **2006**, https://www.un.org/waterforlifedecade/scarcity.shtml (accessed: November 2014).
[5] M. Gao, L. Zhu, C. K. Peh, G. W. Ho, *Energy Environ. Sci.* **2019**, *12*, 841.
[6] C. Li, Y. Goswami, E. Stefanakos, *Renew. Sustainable Energy Rev.* **2013**, *19*, 136.
[7] Z. Wang, Y. Liu, P. Tao, Q. Shen, N. Yi, F. Zhang, Q. Liu, C. Song, D. Zhang, W. Shang, T. Deng, *Small* **2014**, *10*, 3234.
[8] R. Chen, K. Zhu, Q. Gan, Y. Yu, T. Zhang, X. Liu, M. Ye, Y. Yin, *Mater. Chem. Front.* **2017**, *1*, 2620.
[9] C. Liu, J. Huang, C.-E. Hsiung, Y. Tian, J. Wang, Y. Han, A. Fratalocchi, *Adv. Sustainable Syst.* **2017**, *1*, 1600013.
[10] Y. Zeng, K. Wang, J. Yao, H. Wang, *Chem. Eng. Sci.* **2014**, *116*, 704.
[11] Y. Wang, L. Zhang, P. Wang, *ACS Sustainable Chem. Eng.* **2016**, *4*, 1223.
[12] Y. Liu, J. Chen, D. Guo, M. Cao, L. Jiang, *ACS Appl. Mater. Interfaces* **2015**, *7*, 13645.
[13] G. Zhu, J. Xu, W. Zhao, F. Huang, *ACS Appl. Mater. Interfaces* **2016**, *8*, 31716.
[14] L. Zhou, Y. Tan, J. Wang, W. Xu, Y. Yuan, W. Cai, S. Zhu, J. Zhu, *Nat. Photonics* **2016**, *10*, 393.
[15] J. Zhou, Y. Gu, P. Liu, P. Wang, L. Miao, J. Liu, A. Wei, X. Mu, J. Li, J. Zhu, *Adv. Funct. Mater.* **2019**, *29*, 1903255.
[16] N. Xu, X. Hu, W. Xu, X. Li, L. Zhou, S. Zhu, J. Zhu, *Adv. Mater.* **2017**, *29*, 1606762.
[17] Y. Wang, C. Wang, X. Song, M. Huang, S. K. Megarajan, S. F. Shaukat, H. Jiang, *J. Mater. Chem. A* **2018**, *6*, 9874.
[18] F. Zhao, X. Zhou, Y. Shi, X. Qian, M. Alexander, X. Zhao, S. Mendez, R. Yang, L. Qu, G. Yu, *Nat. Nanotechnol.* **2018**, *13*, 489.
[19] H. Ghasemi, G. Ni, A. M. Marconnet, J. Loomis, S. Yerci, N. Miljkovic, G. Chen, *Nat. Commun.* **2014**, *5*, 4449.
[20] X. Hu, W. Xu, L. Zhou, Y. Tan, Y. Wang, S. Zhu, J. Zhu, *Adv. Mater.* **2017**, *29*, 1604031.
[21] H. D. Kiriarachchi, F. S. Awad, A. A. Hassan, J. A. Bobb, A. Lin, M. S. El-Shall, *Nanoscale* **2018**, *10*, 18531.
[22] Z. Liu, H. Song, D. Ji, C. Li, A. Cheney, Y. Liu, N. Zhang, X. Zeng, B. Chen, J. Gao, Y. Li, X. Liu, D. Aga, S. Jiang, Z. Yu, Q. Gan, *Global Challenges* **2017**, *1*, 1600003.
[23] World Coal Association, Where Coal is Found, https://www.worldcoal.org/ (accessed: January 2020).
[24] U. E. P. Agency, https://web.archive.org/web/20081201120536/http://www.epa.gov/radtown/coal-plant.html (accessed: April 2006).
[25] Research Center for Superhard Materials, Database of X-ray diffraction spectra, http://tisncm.ru/index_eng.html (accessed: January 1997).
[26] Z. Song, C. Kuenzer, *Int. J. Coal Geol.* **2017**, *171*, 142.
[27] C. Ezeakacha, A. Rabbani, S. Salehi, A. Ghalambor, in *SPE International Conference and Exhibition on Formation Damage Control*, Society of Petroleum Engineers, Dallas, TX **2018**, p. SPE-189509-MS.
[28] C. Chen, Y. Kuang, L. Hu, *Joule* **2019**, *3*, 683.
[29] X. Li, G. Ni, T. Cooper, N. Xu, J. Li, L. Zhou, X. Hu, B. Zhu, P. Yao, J. Zhu, *Joule* **2019**, *3*, 1798.
[30] H. Kou, Z. Liu, B. Zhu, D. K. Macharia, S. Ahmed, B. Wu, M. Zhu, X. Liu, Z. Chen, *Desalination* **2019**, *462*, 29.
[31] Y. Li, T. Gao, Z. Yang, C. Chen, W. Luo, J. Song, E. Hitz, C. Jia, Y. Zhou, B. Liu, B. Yang, L. Hu, *Adv. Mater.* **2017**, *29*, 1700981.
[32] Y. Zhang, S. K. Ravi, J. V. Vaghasiya, S. C. Tan, *iScience* **2018**, *3*, 31.
[33] X. Wang, X. Li, G. Liu, J. Li, X. Hu, N. Xu, W. Zhao, B. Zhu, J. Zhu, *Angew. Chem.* **2019**, *131*, 12182.
[34] WHO Chronicles, *Guidelines for Drinking Water Quality*, **2011**, (accessed: April 2011).
[35] B. Hong, E. Slatick, *Quarterly Coal Report* **1994**, https://www.eia.gov/coal/production/quarterly/co2_article/co2.html (accessed: April 1994).
[36] World Bank, *The Role of Desalination in an Increasingly Water-Scarce World*, **2019**, https://hdl.handle.net/10986/31416 (accessed: March 2019).
[37] I.R.E.A. (IRENA), Renewable power generation costs in 2019, **2019**, https://www.irena.org/publications/2020/Jun/Renewable-Power-Costs-in-2019 (accessed: June 2020).
[38] Infographics, Mapped: The world's coal power plants, https://www.carbonbrief.org/mapped-worlds-coal-power-plants (accessed: March 2020).